

Evolution of oxygen and nitrogen abundances and nitrogen production mechanism in massive star-forming galaxies

Yu-Zhong Wu¹ and Shuang-Nan Zhang^{1,2}

ABSTRACT

Utilizing the observational data of 55,318 star-forming galaxies (SFGs) selected from the catalog of MPA-JHU emission-line measurements for the SDSS DR8, we investigate the galaxy downsizing effect of their O and N enrichments, and the nitrogen production mechanism in them. We show the redshift evolution of O and N abundances and specific star formation rates for different galaxy mass ranges, demonstrating the galaxy downsizing effect caused by less massive progenitors of less massive galaxies. The O and N abundances do not remain constant for different galaxy mass ranges, and the enrichment (and hence star formation) decreases with increasing galaxy stellar mass. We find evidence of the O enrichment for galaxies with stellar masses $M_* > 10^{11.0}$ (in units of M_\odot), i.e. $\Delta(\log(\text{O}/\text{H})) \sim 0.10$ and $\Delta(\log(\text{N}/\text{H})) \sim 0.28$ from redshift 0.023 to 0.30. Based on the evolutionary schematic model of N/O ratios in Coziol et al., who proposed the scheme that the production of nitrogen is the consequence of a sequence of bursts in SFGs, we conclude that the nitrogen production is dominated by the intermediate-mass stars, which dominate the secondary synthesis in SFGs. However, for galaxies with $M_* > 10^{10.35}$ we find evidence of enhanced N/O abundance ratios, which are significantly above the secondary synthesis line. This suggests that outflows of massive stars, which deplete oxygen efficiently, are more important in massive galaxies. Finally we find an excellent linear relation between M_* and $\log(\text{N}/\text{O})$, indicating that the N/O abundance ratio is a good indicator of the stellar mass in a SFG and may be used as a standard candle for studying cosmology, if confirmed with further studies.

Subject headings: galaxies: abundances — galaxies: starburst — galaxies: statistics

¹Key Laboratory for Particle Astrophysics, Institute of High Energy Physics, Chinese Academy of Sciences, 19B Yuquan Road, Beijing 100049 (zhangsn@ihep.ac.cn)

²National Astronomical Observatories, Chinese Academy of Sciences, 20A Datun Road, Beijing 100012

1. INTRODUCTION

The metallicity of a galaxy is a crucial parameter for understanding its formation and evolution. The element abundances of the interstellar medium (ISM) are obtained by tracers of the chemical compositions of stars and gas within a galaxy. Optical emission lines from HII regions have long been regarded as the principal tools of gas-phase chemical diagnostics in galaxies (Aller 1942; Peimbert 1975; Pagel 1986; de Robertis 1987; Liang et al. 2006). Since estimating metallicities needs theoretical models, empirical calibrations or a combination of both (Kewley & Dopita 2002; Kewley & Ellison 2008), we have different methods to obtain metallicities.

Assuming a classical HII region model, the ratio of the auroral line [O III] λ 4363 to a lower excitation line such as [O III] λ 5007, can be used to determine the electron temperature of the gas, which is then converted into the metallicity of the gas (Osterbrock 1989). The method of using the observed line ratios to infer directly the electron temperatures and to estimate metallicities in galaxies is known as “direct T_e method” (Pagel et al. 1992; Skillman & Kennicutt 1993). This method is generally regarded as the most accurate abundance measurement for estimating metallicities in galaxies. It, however, has two disadvantages. In most instances, [O III] λ 4363 line is too weak to be detected. It is well known that in metal-rich galaxies, the electron temperature decreases (as the cooling is via metal lines) and the auroral lines eventually become too faint to be measured, when the metallicity increases (Yin et al. 2007). In addition, in low-metallicity galaxies, the oxygen abundance is usually underestimated by the [O III] λ 4363 diagnostic in low-metallicity galaxies (Kobulnicky et al. 1999).

Due to the above reasons, photoionization models are used instead for estimating abundances of high metallicity star-forming galaxies (SFGs). The most wide and common method used is the R23 method proposed by Pagel et al. (1979) and Alloin et al. (1979); the oxygen indicator $R_{23} = ([\text{O II}] \lambda\lambda 3727, 3729 + [\text{O III}] \lambda\lambda 4959, 5007) / \text{H}\beta$ suggested by Pagel et al. (1979) is widely accepted and used. Moreover, the relation between the line intensities of strong oxygen lines and the oxygen abundance has been calibrated by photoionization models (e.g., Edmunds & Pagel 1984; McCall et al. 1985; Dopita & Evans 1986; Kobulnicky et al. 1999; Kewley & Dopita 2002). However, it has one problem that the relationship between R_{23} and $12 + \log(\text{O}/\text{H})$ is double valued, which shows the transition between the upper metal-rich branch and the lower metal-poor branch occurring near $12 + \log(\text{O}/\text{H}) \sim 8.4$ (Liang et al. 2006).

With the releases of catalogues of several large spectral surveys, especially the Sloan Digital Sky Survey (SDSS) that has released a large number of spectral data, the number of good-quality spectra of emission-line galaxies has increased dramatically (York et al. 2000).

These open a new era of utilizing the large survey spectra to study the evolution of O and N abundances in galaxies. Using the line flux measurements of SDSS spectra, Thuan et al. (2010) not only found the evolution of O and N abundances in galaxies with different stellar masses, but also found evidence for galaxy downsizing that metal enrichment shifts from higher-mass galaxies at early cosmic times to lower-mass ones at later epochs (Cowie et al. 1996).

In the last decade, the evolution of the mass-metallicity relation of galaxies with redshift has been investigated by several groups (Lilly et al. 2003; Savaglio et al. 2005; Erb et al. 2006; Cowie & Barger 2008; Maiolino et al. 2008; Lamareille et al. 2009; Lara-López et al. 2009). In these studies, they used different methods to obtain O abundances and found the O abundance change of SFGs, with $\Delta(\log(\text{O}/\text{H})) \sim 0.3$ or lower. In addition, Thuan et al. (2010) have paid attention to the redshift evolution of N abundances in galaxies and have shown two advantages for studying the chemical evolution of galaxies. Firstly, at $12 + (\log(\text{O}/\text{H})) \gtrsim 8.3$, nitrogen abundance change with redshift has a larger amplitude than that of oxygen. Then, compared with oxygen production, the nitrogen production has a time delay (Maeder 1992; van den Hoek & Groenewegen 1997; Pagel 1997), and it can give some limits for the chemical evolution of galaxies. Using a large sample of galaxies in the Great Observatories Origins Deep Survey-North (GOODS-N), Cowie & Barger (2008) found that star formation ceases in most massive galaxies (with stellar masses $M_* > 10^{11}$ in units of M_\odot) at $z < 1.5$. Thuan et al. (2010) also found $\Delta(\log(\text{O}/\text{H})) = 0$ for massive galaxies with $M_* > 10^{11}$.

Although the evolution of O and N abundances of galaxies with redshift has been widely studied, we still cannot fully understand the downsizing effect (i.e., some disputes for the origin of the downsizing; Poggianti et al. 2004; Bundy et al. 2006). Moreover, some studies seem to show no signs of the evolution of O abundance with redshift in most massive galaxies ($M_* > 10^{11}$). Therefore, we utilize the MPA-JHU DR8 release of spectral measurements to investigate these issues.

In this work, we first present the galaxy downsizing effect; we then show evidence of the O enrichment for galaxies with $M_* > 10^{11.0}$. On the basis of the evolutionary schematic model of N/O ratios, we can clarify the nitrogen production mechanisms in SFGs.

For the line fluxes, we use the following notations throughout this paper: $R_2 = I_{[\text{O II}]\lambda 3727 + \lambda 3729} / I_{\text{H}\beta}$, $R_3 = I_{[\text{O III}]\lambda 4959 + \lambda 5007} / I_{\text{H}\beta}$, $N_2 = I_{[\text{N II}]\lambda 6548 + \lambda 6584} / I_{\text{H}\beta}$, $R_{23} = R_2 + R_3$.

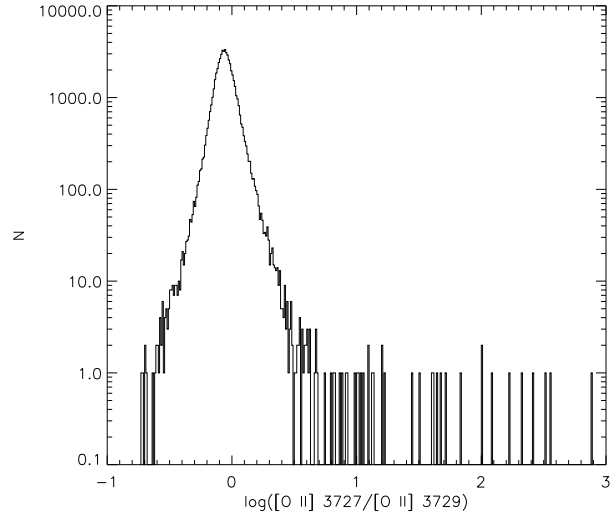


Fig. 1.— The distribution of $[\text{O II}] \lambda 3727 / [\text{O II}] \lambda 3729$ flux ratios.

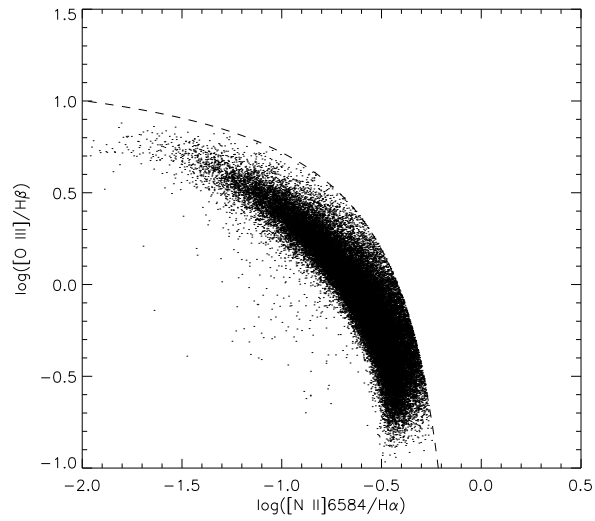


Fig. 2.— Traditional diagnostic diagram. The dashed curve on the diagram is the Kauffmann et al. (2003a) semi-empirical lower boundary for the star-forming galaxies.

2. THE SAMPLE and DATA

The catalog of MPA-JHU emission-line measurements for the SDSS Data Release 8 (DR8) is chosen as our primary sample. The measurements are available for 1,843,200 different spectra. Compared to the previous DR4 release used for a similar study (Wu, Zhao, & Meng 2011), this represents a significant extension in size and a number of improvements in the data.

The MPA-JHU DR8 release of spectral measurements provides many parameters, such as the redshift, galaxy stellar mass, and various emission line measurements. These data are available online at the following address: <http://www.sdss3.org/dr8/spectro/galspec.php>. We initially select 71,888 objects from the above sample with the criterion of $S/N > 5$ for the redshift, $H\beta$ $\lambda 4861$, $H\alpha$ $\lambda 6563$, $[O\ II]$ $\lambda 3727$, $[O\ II]$ $\lambda 3729$, $[N\ II]$ $\lambda 6584$, $[O\ III]$ $\lambda 5007$, $[O\ I]$ $\lambda 6300$, $[S\ II]$ $\lambda 6717$, and $[S\ II]$ $\lambda 6731$ lines. In addition, we have excluded these galaxies for their FLAG keywords of zero and -9999.0 in SFR and sSFR.

Due to that $3800\text{\AA} - 9300\text{\AA}$ is the wavelength range of the SDSS spectra, the range of redshifts in our nearby galaxies can be determined. If the $[O\ II]$ $\lambda\lambda 3727, 3729$ emission lines are not out of the observed range, then the lower limit of redshifts in our nearby galaxies is $z \approx 0.023$. As shown in Fig. 1, a tiny fraction of the objects show anomalously large $[O\ II]$ $\lambda 3727/[O\ II]$ $\lambda 3729$ ratios; we thus exclude 30 objects with $[O\ II]$ $\lambda 3727/[O\ II]$ $\lambda 3729 > 10$. If the $[S\ II]$ $\lambda\lambda 6717, 6731$ emission lines are not out of the observed range, then the upper limit of redshifts in our nearby galaxies is $z \approx 0.33$ (Pilyugin & Thuan 2011).

The SFG sample presented in Fig. 2 is based on the BPT diagram (Baldwin et al. 1981; Veilleux & Osterbrock 1987), and the separation line between AGNs and SFGs proposed by Kauffmann et al. (2003a) is the criterion of the SFG sample. We select all the objects which reside in the lower left corner of the Kauffmann et al. (2003a) line as our SFG sample, and we exclude the objects with redshift $z > 0.30$. Therefore, we obtain the galaxy sample with 55,318 objects.

In addition to the redshift of each galaxy from the release of the MPA-JHU DR8 catalog, the release also provides the stellar masses of all galaxies based on the fits to the photometry following the philosophy of Kauffmann et al. (2003a) and Salim et al. (2007); the stellar masses are FITS binary tables with keys MEDIAN. The galaxy stellar masses come all from the MPA-JHU DR8 catalog in this paper. In addition, the specific star formation rate (sSFR), taken as the median of the PDF of the sSFR for each SFG, is also added for completeness.

3. Metallicity calibrations

In this section, we estimate the oxygen and nitrogen abundances utilizing both emission-line fluxes and recent calibrations. The oxygen abundances of the sample galaxies are estimated using the R_{23} method (Pilyugin et al. 2006; Pilyugin et al. 2010; Zahid et al. 2012),

$$R_{23} = R_2 + R_3. \quad (1)$$

We adopt the calibration of Tremonti et al. (2004),

$$12 + \log(\text{O}/\text{H}) = 9.185 - 0.313x - 0.264x^2 - 0.321x^3, \quad (2)$$

where x is $\log R_{23}$.

The $\log(\text{N}/\text{O})$ abundance ratios of these SFGs are estimated by using the algorithm given by Thurston et al. (1996),

$$t_{\text{II}} = 6065 + 1600x + 1878x^2 + 2803x^3, \quad (3)$$

where t_{II} is the [N II] temperature (in units of 10^4 K), and x is $\log R_{23}$.

Based on a five-level atom calculation, Pagel et al. (1992) given a convenient formula:

$$\log \frac{\text{N}^+}{\text{O}^+} = \log \frac{N_2}{R_2} + 0.307 - 0.02 \log t_{\text{II}} - \frac{0.726}{t_{\text{II}}}. \quad (4)$$

Here, we take $N_2 = 1.33$ [N II] $\lambda 6584$ instead of the standard $N_2 = [\text{N II}] \lambda 6548 + [\text{N II}] \lambda 6584$, because the measurements of the [N II] $\lambda 6548$ line are less reliable than those of the [N II] $\lambda 6584$ line (Thuan et al. 2010). To derive N/O, we make the following assumption,

$$\frac{\text{N}^+}{\text{O}^+} = \frac{\text{N}}{\text{O}}. \quad (5)$$

With regard to the accuracy of this assumption, some discussions were given by Vila-Costas & Edmunds (1993), and Thurston et al. (1996) suggested that this assumption is fairly accurate.

The above calibration and procedure of obtaining the O abundance and the N/O abundance ratio together for SFGs have been widely used in literature, e.g., Liang et al. (2006), Mallery et al. (2007), and Lara-López et al. 2009. The total N abundance can then be obtained from

$$\log \frac{\text{N}}{\text{H}} = \log \frac{\text{N}}{\text{O}} + \log \frac{\text{O}}{\text{H}}. \quad (6)$$

4. RESULTS AND DISCUSSION

In this section, we firstly present the galaxy downsizing effect, i.e., enrichment ceases in higher-mass galaxies at earlier times and shifts to lower-mass galaxies at later epochs (Pilyugin & Thuan 2011); we show that both enrichment rates (i.e. slopes in Figs 3 – 6) and sSFRs (in Fig. 7) decrease between redshift 0.3 and 0.023, as well as that abundances at $z \sim 0.023$ increase, but sSFRs decrease with the galaxy stellar mass growth. Then we demonstrate the O and N enrichments for $M_* > 10^{11.0}$. Finally we discuss the relation of the nitrogen productions between intermediate-mass stars and massive stars using the model proposed by Coziol et al. (1999) in SFGs.

4.1. The Galaxy Downsizing Effect

In Fig. 3, we show the redshift evolution of O and N abundances for different galaxy mass ranges; their contours are presented in Fig. 4. In each panel, the red and black points represent O and N abundances of SFGs at different redshifts, respectively, and the best least-squares fits are shown by the solid lines. The upper panel shows that the N and O abundance variations with redshift in galaxies with $M_* < 10^{9.5}$. This indicates that these galaxies have not reached a high astration level some 3 Gyr ago and are experiencing intense star formation in their evolution processes. This is consistent with the result of Pilyugin & Thuan (2011).

From Fig. 3 and Table 1, we can see that the slope for O abundance increases from -1.08 to -0.33 when the stellar mass increases from $M_* < 10^{9.5}$ to $M_* < 10^{11.0}$, as seen visually in Fig. 4. This indicates that the O enrichment (or star formation) decreases with the galaxy stellar mass growth (see Table 1). This demonstrates the galaxy downsizing effect, consistent with Pilyugin & Thuan (2011) who noted that O enrichment seems to decrease slowly with increasing galaxy stellar mass. In addition, the O and N abundances do not remain constant between different galaxy mass ranges, and O abundance at $z \sim 0.023$ increases from 8.76 to 9.12 with increasing galaxy stellar mass. This is inconsistent with the result of Pilyugin & Thuan (2011), who noted that O abundances are always ~ 8.5 for different stellar mass galaxies at $z \sim 0.023$. Moreover, the galaxies with the same stellar mass range present significantly larger N enrichment than O enrichment (see Table 1), which confirms the result of Thuan et al. (2010). It is also noticeable that the difference between $12+\log(\text{O}/\text{H})$ and $12+\log(\text{N}/\text{H})$ decreases with the galaxy mass, indicating that the O enrichment lags behind the N enrichment as galaxies grow, which will be extensively discussed in section 4.4.

In Fig. 5, we show the redshift evolution of N/O abundance ratios for different galaxy

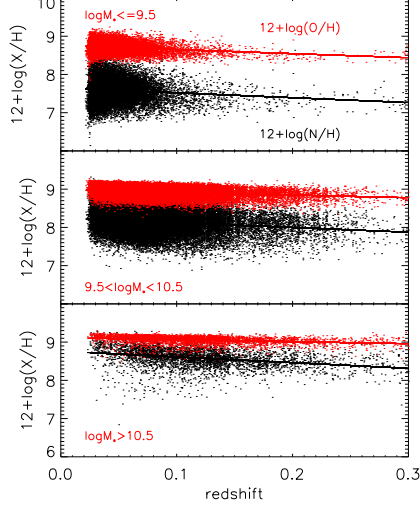


Fig. 3.— Oxygen and nitrogen abundances as a function of redshift for those galaxies with $M_* < 10^{9.5}$, $10^{9.5} - 10^{10.5}$, and $> 10^{10.5}$. Oxygen and nitrogen abundances are shown by red and black points, respectively. The red and black solid lines are the best least-squares fits for these data.

Table 1: Summary of nitrogen and oxygen abundances.

Galaxy mass	sample size	log(N/O)			12+log(N/H)			12+log(O/H)		
		a	b	c	a	b	c	a	b	c
(1)	(2)	(3)	(4)	(5)	(6)	(7)	(8)	(9)	(10)	(11)
$\log M_* \leq 9.5$	17226	-1.11	-0.22	0.06	7.65	-1.30	0.36	8.76	-1.08	0.30
$9.5 < \log M_* \leq 10.5$	34100	-0.74	-0.57	0.16	8.25	-1.27	0.35	8.99	-0.71	0.20
$\log M_* > 10.5$	3992	-0.36	-1.08	0.30	8.76	-1.64	0.45	9.12	-0.56	0.16
$\log M_* > 11.0$	284	-0.33	-0.67	0.19	8.77	-1.01	0.28	9.10	-0.33	0.09

NOTE: Col.(1): Galaxy mass. Col.(2): the sample size of SFGs. Cols.(3)-(5), (6)-(8), and (9)-(11): For each sample of the log(N/O), 12+log(N/H), and 12+log(O/H). “a” are the values of log(N/O), 12+log(N/H), and 12+log(O/H) at $z \sim 0.023$, respectively. “b” are slopes (enrichment rates) of log(N/O), 12+log(N/H), and 12+log(O/H) between $z \sim 0.3$ and $z \sim 0.023$, respectively. “c” are $\Delta(\log(N/O))$, $\Delta(12 + \log(N/H))$, and $\Delta(12 + \log(O/H))$ between $z \sim 0.3$ and $z \sim 0.023$, respectively.

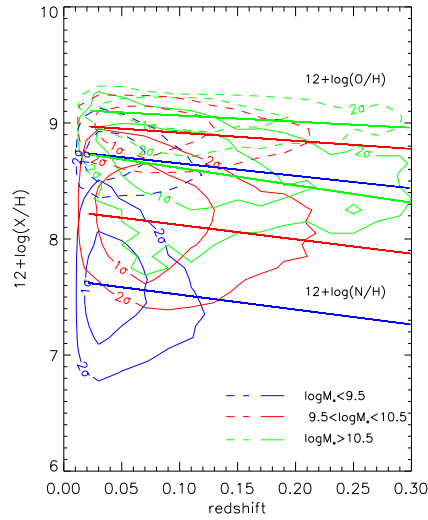


Fig. 4.— Contours of oxygen and nitrogen abundances as a function of redshift for those galaxies with $M_* < 10^{9.5}$, $10^{9.5} - 10^{10.5}$, and $> 10^{10.5}$. 1σ and 2σ correspond to the 1σ and 2σ regions of the Gaussian distribution for both redshift and $12+\log(\text{O}/\text{H})$ or $12+\log(\text{N}/\text{H})$. The dashed and solid curves are the contours of $12+\log(\text{O}/\text{H})$ and $12+\log(\text{N}/\text{H})$, respectively. The blue, red, and green lines (both solid and dashed) display those galaxies with $M_* < 10^{9.5}$, $10^{9.5} - 10^{10.5}$, and $> 10^{10.5}$, respectively. The straight lines (both solid and dashed) are the best least-squares fits for these data.

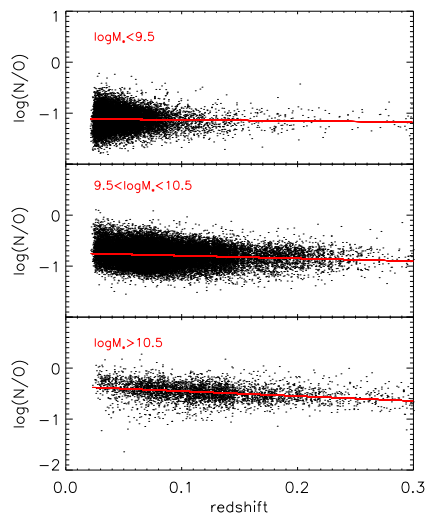


Fig. 5.— Nitrogen-to-oxygen abundance ratios as a function of redshift for those galaxies with $M_* < 10^{9.5}$, $10^{9.5} - 10^{10.5}$, and $> 10^{10.5}$. These abundance ratios are shown by black points. The red solid lines are the best least-squares fits for these data.

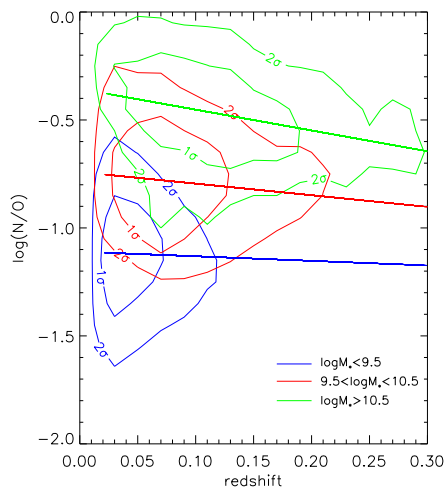


Fig. 6.— Contours of nitrogen-to-oxygen abundance ratios as a function of redshift for those galaxies with $M_* < 10^{9.5}$, $10^{9.5} - 10^{10.5}$, and $> 10^{10.5}$. 1σ and 2σ correspond to the 1σ and 2σ regions of the Gaussian distribution for both redshift and $\log(N/O)$. The solid lines are the best least-squares fits for these data.

mass ranges; their contours are presented in Fig. 6. In the upper panel of Fig. 5, the sample size of galaxies with $M_* < 10^{9.5}$ is 17226, and the N/O abundance ratio at $z \sim 0.023$ is -1.11 . In the middle and lower panels of Fig. 5, the sample sizes of galaxies with M_* of $10^{9.5} - 10^{10.5}$ and $> 10^{10.5}$ are 34100 and 3992, respectively, and the N and O abundances at $z \sim 0.023$ are -0.74 and -0.36 , respectively. These indicate that the N/O abundance ratio increases with increasing galaxy stellar mass. This is in good agreement with the relation between N/O and the stellar mass of Pérez-Montero & Contini (2009).

Fig. 7 shows the redshift evolution of the specific star formation rate (sSFR) for different galaxy mass ranges. In each panel, the black points represent sSFRs of SFGs at different redshifts, and the best least-squares fits are shown by the solid (red) lines. From Fig. 7, we find that the slopes for sSFRs decrease from 6.39 to 4.39 and then to 3.58, and the intercepts for sSFRs at $z \sim 0.023$ decrease from -9.70 to -10.00 and then to -10.11 with galaxy stellar mass from $M_* < 10^{9.5}$ to $10^{9.5} - 10^{10.5}$ and then to $> 10^{10.5}$. This is consistent with Fig. 3 of Pilyugin et al. (2013). Clearly in this low redshift range the sSFRs of less massive galaxies are on average always higher than that of more massive galaxies, explaining the galaxy downsizing effect shown in Fig. 3 or 4. In other words, less massive galaxies are less massive because of their less massive progenitors, despite of their higher sSFRs.

4.2. The O and N Enrichments for Galaxies with $M_* > 10^{11.0}$

In this section, we firstly present the evidence of the O and N enrichments for galaxies with $M_* > 10^{11.0}$. Then we show the redshift evolution of N/O abundance ratios for galaxies with $M_* > 10^{11.0}$. Finally, we discuss the O and N enrichments for these most massive galaxies.

In Fig. 8, we show the O and N enrichments and the redshift evolution of N/O abundance ratios for galaxies with $M_* > 10^{11.0}$. The sample size of galaxies with $M_* > 10^{11.0}$ is 284. The upper panel shows evidence of the N and O enrichments. The slopes are -0.33 and -1.01 for O and N abundances, respectively, and the N/O abundance ratios at $z \sim 0.023$ are 9.10 and 8.77, respectively. The lower panel shows the redshift evolution of N/O abundance ratios. The slope is -0.67 for N/O abundance ratios. In Fig. 13 of Thuan et al. (2010), the O and N enrichments were shown for galaxies with M_* of $10^{10.0} - 10^{10.3}$; however, the O and N enrichments were not seen for galaxies with M_* of $10^{11.2} - 10^{11.5}$.

Employing data of the VIMOS VLT Deep Survey, Lamareille et al. (2009) obtained the mass-metallicity relation of SFGs and have found that the galaxies of $10^{10.2}$ show a larger O enrichment than those of $10^{9.4}$. In addition, Lara-López et al. (2009) have studied

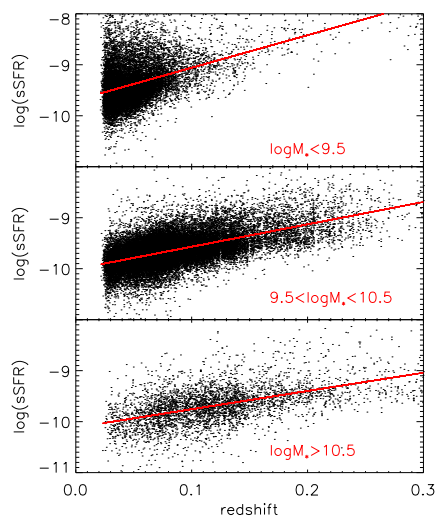


Fig. 7.— Specific star formation rate (sSFR) as a function of redshift for galaxies with $M_* < 10^{9.5}$, $10^{9.5} - 10^{10.5}$, and $> 10^{10.5}$. The red solid lines are the best least-squares fits.

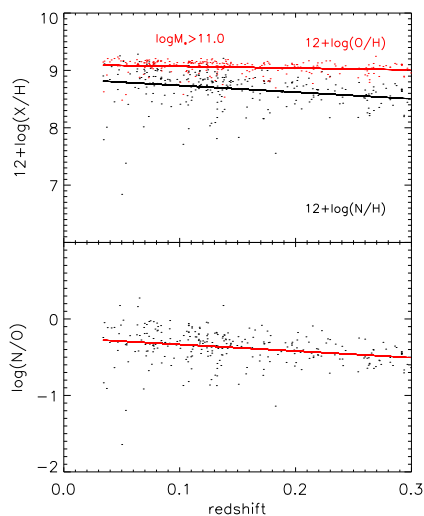


Fig. 8.— O and N enrichments and N/O abundance ratio as a function of redshift for galaxies with $M_* > 10^{11.0}$. Oxygen and nitrogen abundances are shown by red and black points, respectively, in the upper panel. The abundance ratios are shown by black points in the lower panel. The red and black solid lines are the best least-squares fits for these data.

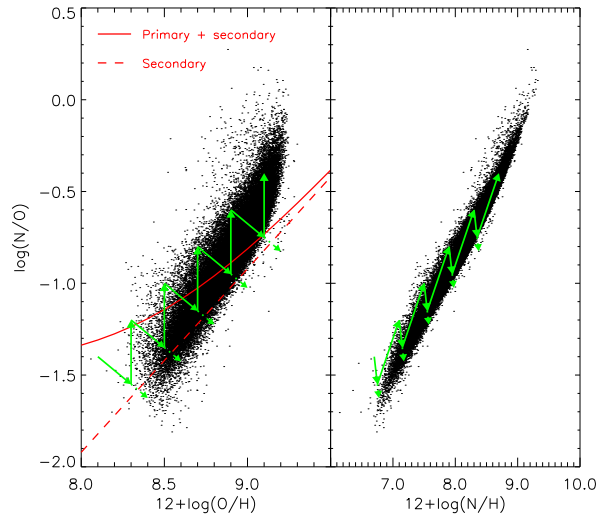


Fig. 9.— Schematic demonstration of the nitrogen productions of intermediate-mass and massive stars in a sequence of bursts. During a cycle, the massive star evolution not only produces the oxygen enrichment, but also produces the nitrogen enrichment; the intermediate-mass star evolution produces only the nitrogen enrichment. In all cycles, the enrichment of the intermediate-mass stars should be larger than that of the massive stars.

the O abundance of relatively massive ($\log(M_*) \geq 10.5$) SFGs from SDSS/DR5 at different redshift intervals from 0.4 to 0.04. They found an oxygen enrichment $\Delta(\log(\text{O}/\text{H})) \sim 0.1$ from redshift 0.4 to 0. From Fig. 9 and Table 1, we can see clearly $\Delta(\log(\text{O}/\text{H})) \sim 0.10$ and $\Delta(\log(\text{N}/\text{H})) \sim 0.28$ from redshift 0.023 to 0.30. Comparing with the above results, we may safely conclude that the O and N are enriched for galaxies with $M_* > 10^{11.0}$.

4.3. The N Production in Star Forming Galaxies

In this section, we first introduce a schematic demonstration of productions of primary and secondary nitrogen in a sequence of bursts (Coziol et al. 1999). Then we show that the nitrogen production of intermediate-mass stars is larger than that of massive stars in SFGs.

Based on the evolutionary schematic model of N/O ratios in Garnett (1990), Coziol et al. (1999) proposed a scheme that the production of nitrogen is the consequence of a sequence of bursts in SFGs. This means that the N abundance and the metallicity increase in SFGs, because these galaxies experience a couple of star formation processes in several cycles. During a cycle, the $12 + \log(\text{O}/\text{H})$ increases due to the evolution of massive stars,

while the N/O ratio decreases (Garnett 1990; Olofsson 1995; Coziol et al. 1999). After ~ 0.4 Gyrs of massive star active onset, the intermediate-mass stars contribute most nitrogen, and the N/O ratio increases sharply, while the $12 + \log(\text{O}/\text{H})$ does not increase.

Utilizing the SDSS DR7 data, Torres-Papaqui et al. (2012) found that the intensity of the bursts seems to result in the chemical differences between the nitrogen-poor and nitrogen-rich SFGs, which is well explained by the sequence of bursts model (Coziol et al. 1999). In addition, the SDSS DR8 data are selected as the SFG sample, and Wu & Zhang (in preparation) found that the metallicity increase on the BPT diagram can be explained by several star formation processes. These suggest that a sequence of bursts model may help to understand the chemical evolution of SFGs.

In Fig. 9, we show the relations of $\log(\text{N}/\text{O})$ versus $12 + \log(\text{O}/\text{H})$ and $12 + \log(\text{N}/\text{H})$, respectively. Generally, the N/O ratio will be constant for primary nucleosynthesis, while this ratio will be a linear correlation for secondary nucleosynthesis. The combination of both primary and secondary nucleosyntheses gives rise to a nonlinear relation (Mallery et al. 2007). During the first cycle, the evolution of massive stars contribute not only the $12 + \log(\text{O}/\text{H})$ increase but also the N/O ratio decrease in the left panel; in the meantime, this process also produces some nitrogen (the right panel in Fig. 9). With the evolution of these galaxies, the massive stars start dying off, and the intermediate-mass stars open large scale nitrogen production (the right panel in Fig. 9), but the oxygen production ceases (the left panel in Fig.9). In the right panel, it can be seen that the nitrogen production of the intermediate-mass stars is larger than that of the massive stars. Therefore, the nitrogen production is dominated by the intermediate-mass stars in SFGs during the first cycle.

The second cycle begins with an increase in the $12 + \log(\text{O}/\text{H})$ and a decreases in the N/O ratio, and this cycle will follow the first cycle regardless of that the star formation process has a lower or higher amplitude (intensity) than that of the first cycle. Actually, some models of successive bursts assume that the bursts will have decreasing intensities (Gerola, Seiden, & Schulman 1980; Krugel & Tutukov 1993; Marconi, Matteucci, & Tosi 1994; Koeppen, Theis, & Hensler 1995; Coziol et al. 1999). However, our result that the nitrogen production is dominated by the intermediate-mass stars in SFGs will not be changed, because the nitrogen production processes of intermediate-mass and massive stars are the same as those of the first cycle.

Regarding relative high-metallicities ($12 + \log(\text{O}/\text{H}) \gtrsim 8.3$) objects, the N/O ratio increases significantly with the O abundance growth. The trend seems to originate from the nitrogen production with metallicity-dependence in both massive and intermediate-mass stars (e.g., Vila-Costas & Edmunds 1993; Pilyugin et al. 2003). Therefore, the nitrogen is generally a secondary element in the metallicity range (Vila-Costas & Edmunds 1993; Henry,

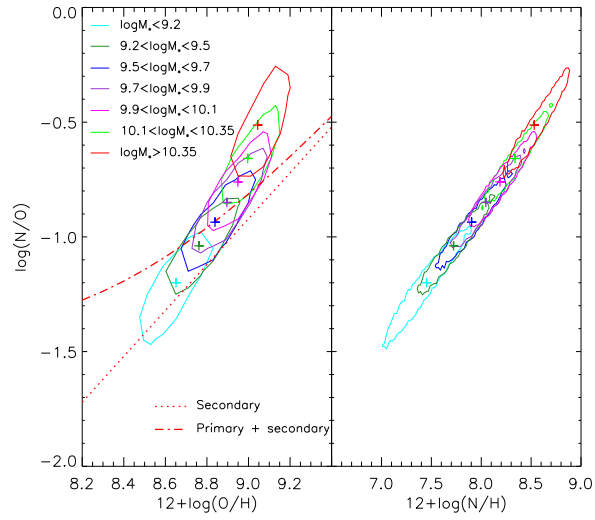


Fig. 10.— Contours of N/O abundance ratios as functions of $12+\log(O/H)$ and $12+\log(N/H)$ for those galaxies with different galaxy mass ranges. 1σ corresponds to the 1σ region of the Gaussian distribution for both $\log(N/O)$, $12+\log(O/H)$, and $12+\log(N/H)$. Seven ‘+’ signs mark the central values of the distributions for these parameters among seven different galaxy mass ranges.

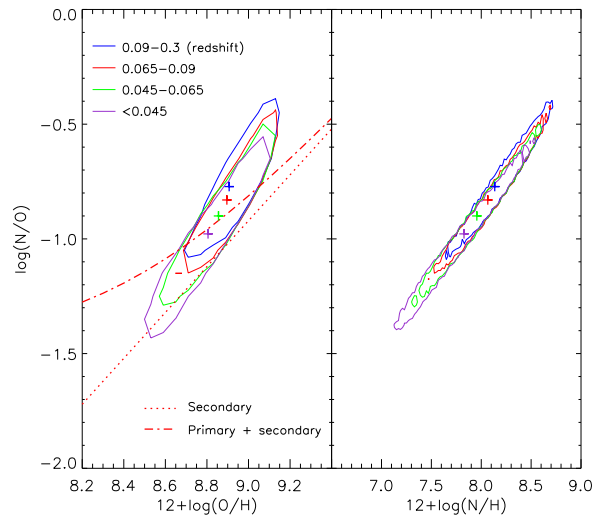


Fig. 11.— Contours of N/O abundance ratios as functions of $12+\log(O/H)$ and $12+\log(N/H)$ for those galaxies with different redshift ranges. 1σ corresponds to the 1σ region of the Gaussian distribution for both $\log(N/O)$, $12+\log(O/H)$, and $12+\log(N/H)$. Four pluses are the central values of the distributions for these parameters among four different redshift ranges.

Edmunds, & Köppen 2000; van Zee & Haynes 2006; López-Sánchez & Esteban 2010). Since primary synthesis is commonly assumed (but not definitely) to confine in intermediate-mass stars, while secondary synthesis could occur in stars of all masses (Renini & Voli 1981; Vila-Costas & Edmunds 1993), our result that the nitrogen production is dominated by the intermediate-mass stars is reasonable. During the main sequence (MS), intermediate mass stars burn hydrogen through the CNO cycle. The conversion of almost all central C^{12} into N^{14} is the consequence of the CNO cycle (Smiljanic et al. 2006). In addition, intermediate-mass stars seem most likely to contribute, during the asymptotic giant branch, the CNO-processed material (Cannon et al. 1998).

In term of initial mass function (IMF), equations 1 and 2 in Kroupa (2001) show that a mean stellar mass $\langle m \rangle = 0.36 M_{\odot}$ for stars with $0.01 \leq m \leq 50 M_{\odot}$, and 5.7 % ‘intermediate-mass (IM) stars’ ($1.0-8.0 M_{\odot}$) contribute 34 % mass, and 0.37 % ‘O’ stars ($>8.0 M_{\odot}$) contribute 17 % mass (Kroupa 2001). Therefore intermediate-mass stars can contribute twice as much mass as massive star in SFGs. This is consistent intermediate-mass stars dominate the nitrogen production in SFGs.

4.4. Enhanced N/O ratio in massive galaxies

However, most of the galaxies in our sample are located significantly above the secondary synthesis line, which has been proposed to dominate the total synthesis of N/O. It is evident that the last arrows that marks the nitrogen production by the intermediate-mass stars in both panels point to the direction of the observed N/O enhancement. This means that no O abundance enhancement is needed for the following star-forming processes. This is inconsistent with Coziol et al. (1999), who suggested that the sum of the vectors of alternating oxygen (by massive stars) and nitrogen (by intermediate-mass stars) converges to the secondary synthesis line. Due to the existence of the outflow/winds, the separation in Fig. 9 may originate from the galactic wind driven by the starburst (Strickland, Ponman, & Stevens 1997; Moran, Lehnert, & Helfand 1999). The outflow will preferentially deplete the oxygen, and nitrogen will remain at its ISM value at the time of the starburst/wind (Lehnert & Heckman 1996; Heckman 2003; Torres-Papaqui et al. 2012). Therefore, the outflow effect may result in the separation of the metallicities of the galaxies from the secondary + primary chemical evolution model of Vila-Costas & Edmunds (1993).

In order to understand the above discrepancy, in Figs 10 and 11 we show their contours and central values (with ‘+’ sign) for different galaxy mass and redshift ranges. Each contour includes 68.3% of the total galaxies for this subsample; all subsamples have almost an equal size in each Figure. Fig. 10 shows clearly that larger mass galaxies show more significant

deviations of N/O abundance ratio above the secondary synthesis line. This is in good agreement with the relation between N/O abundance ratio and O abundance with the stellar mass of Amorín, Pérez-Montero, & Vílchez (2010). Fig. 11 shows that higher redshift galaxies have statistically larger N/O abundance ratios than lower redshift ones. Using a good indicator of the stellar age, Kauffmann et al. (2003b) displayed a correlation between the $D_n(4000)$ index and stellar mass; this relation indicates that massive galaxies seem to be older (Tremonti et al. 2004). This means that higher redshift and more massive galaxies have started their nitrogen enrichment earlier; this is another manifestation of the downsizing effect. Since the N abundance enrichment process is not accompanied with any significant oxygen enrichment, we conclude that the outflows of massive stars, which deplete oxygen efficiently, are more significant in massive galaxies.

In Table 2, we list the sample size, mean and median values of M_* , $\log \frac{N}{O}$, $12 + \log \frac{N}{H}$ and $12 + \log \frac{O}{H}$ of these galaxies in each subsample shown in Figs 10 and 11; in each case, the mean and median values are approximately the same. In Fig 12, we show the relations between the median values of M_* and $\log \frac{N}{O}$, $12 + \log \frac{N}{H}$ and $12 + \log \frac{O}{H}$, respectively; a linear fit to each relation is also shown as the dashed line. Clearly a good linear relation exists between $\log M_*$ and $\log \frac{N}{O}$, i.e.,

$$\log \frac{N}{O} = -5.09 + 0.43 \log M_*, \quad (7)$$

suggesting that N/O abundance ratio is a statistically excellent indicator of the mean/median stellar mass of a sample of SFG. Since M_* is derived from the total stellar lights of a galaxy, a cosmological model (luminosity distance) must be assumed when calculating M_* from the multi-band photometric data. The ability of predicting reliably M_* with Equation (7) from the observed N/O abundance ratio, which is cosmological model independent, suggests that the relation in Equation (7) can be used a standard candle to study cosmology. The parameters (slope and intercept) in Equation (7) are now determined with a given cosmological model in the catalog, thus cannot be used directly to study alternative cosmological models. However, we can use the observed SNe Ia, which are excellent standard candles, to calibrate the relation in Equation (7), in a model-independent way similar to that the method of calibrating several luminosity relations of gamma-ray bursts (Liang et al. 2008, 2010). Since the relationship in equation (7) is derived using only the median values of N/O abundance ratio, its statistical robustness should be carefully studied in the future with, e.g. the method of Kelly (2007). Finally, this relationship needs to be tested in a broader redshift range before it is applied for cosmological studies. However further more detailed discussion on this subject is beyond the scope of this present work and will be presented elsewhere.

With the observational data of 55,318 SFGs selected from the catalog of MPA-JHU emission-line measurements for the SDSS DR8, we find evidence of the galaxy downsizing

effect, the O and N enrichments for galaxies with stellar masses larger than $10^{11.0}$, and the nitrogen production dominated by the intermediate-mass stars in SFGs. We summarize our main results below.

(1) We show the redshift evolution of O and N abundances for different galaxy mass ranges, and it presents the galaxy downsizing effect, consistent with Pilyugin & Thuan (2011). We also show that in this low redshift range the sSFRs of less massive galaxies are on average always higher than that of more massive galaxies, consistent with Pilyugin et al. (2013). This explains the galaxy downsizing effect, i.e., less massive galaxies are less massive because of their less massive progenitors, despite of their higher sSFRs.

(2) The O and N abundances do not remain constant at different galaxy mass ranges, and the enrichment capability (SFRs) decreases with the galaxy stellar mass growth. The O abundance at $z \sim 0.023$ increase from 8.76 to 8.99 and then to 9.12 with increasing galaxy stellar mass, which is inconsistent with the result of Pilyugin & Thuan (2011). Moreover, the galaxies with the same stellar mass range present significantly larger N enrichment than O enrichment (Table 1), which confirms the result of Thuan et al. (2010).

(3) We show the redshift evolution of N/O abundance ratios for different galaxy mass ranges. We find N/O abundance ratios at $z \sim 0.023$ increase with the galaxy stellar mass growth, and the slopes decrease with the galaxy stellar mass growth. This is in good agreement with Pérez-Montero & Contini (2009) and Amorín, Pérez-Montero, & Vílchez (2010).

(4) For the first time we find evidence of the O and N enrichments for galaxies with $M_* > 10^{11.0}$. In contrast to previous conclusion that the most massive galaxies do not show an appreciable enrichment in oxygen, we find $\Delta(\log(\text{O}/\text{H})) \sim 0.10$ and $\Delta(\log(\text{N}/\text{H})) \sim 0.28$ from redshift 0.023 to 0.30 for these very massive galaxies.

(5) We conclude that the nitrogen production is dominated by the intermediate-mass stars, which dominate the secondary synthesis in SFGs.

(6) We find that the N/O abundance ratios of SFGs with $M_* > 10^{10.35}$ are located significantly above the secondary synthesis line. This suggests that outflows of massive stars, which deplete oxygen efficiently, are more important in massive galaxies.

(7) We find an excellent linear relation between M_* and $\log(\text{N}/\text{O})$, indicating that the N/O abundance ratio is good indicator of the stellar mass in a SFG, which may be used as a standard candle for studying cosmology after proper calibration with some other cosmology independent standard candles, such as SNe Ia. However, further careful studies are needed before it is applied to cosmological studies.

Table 2: Summary of SFGs.

Parameters	sample size	log M_*		log(N/O)		12+log(N/H)		12+log(O/H)	
		mean	median	mean	median	mean	median	mean	median
(1)	(2)	(3)	(4)	(5)	(6)	(7)	(8)	(9)	(10)
$\log M_* \leq 9.2$	8734	8.85	8.95	-1.20	-1.21	7.45	7.43	8.65	8.64
$9.2 < \log M_* \leq 9.5$	8492	9.36	9.37	-0.97	-1.04	7.72	7.72	8.81	8.76
$9.5 < \log M_* \leq 9.7$	7974	9.60	9.61	-0.94	-0.94	7.90	7.90	8.84	8.85
$9.7 < \log M_* \leq 9.9$	8487	9.80	9.80	-0.85	-0.85	8.05	8.05	8.90	8.91
$9.9 < \log M_* \leq 10.1$	7551	10.00	9.99	-0.76	-0.77	8.19	8.19	8.95	8.96
$10.1 < \log M_* \leq 10.35$	7286	10.22	10.21	-0.66	-0.67	8.34	8.34	9.00	9.01
$\log M_* > 10.35$	6794	10.58	10.53	-0.53	-0.53	8.51	8.53	9.04	9.06

Parameters	sample size	z		log(N/O)		12+log(N/H)		12+log(O/H)	
		mean	median	mean	median	mean	median	mean	median
$z \leq 0.045$	13732	0.03	0.03	-0.98	-1.01	7.83	7.79	8.80	8.79
$0.045 < z \leq 0.065$	13101	0.06	0.05	-0.90	-0.91	7.95	7.94	8.85	8.86
$0.065 < z \leq 0.09$	13462	0.08	0.08	-0.83	-0.84	8.06	8.08	8.89	8.91
$0.09 < z < 0.3$	15023	0.13	0.12	-0.78	-0.78	8.12	8.16	8.90	8.93

NOTE: Col.(1): M_* or redshift (z) ranges. Col.(2): the subsample size of SFGs. Cols.(3)-(4), (5)-(6), (7)-(8), and (9)-(10): “mean” and “median” are the mean and median values of M_* or z, log(N/O), 12+log(N/H), and 12+log(O/H), respectively, in each subsample.

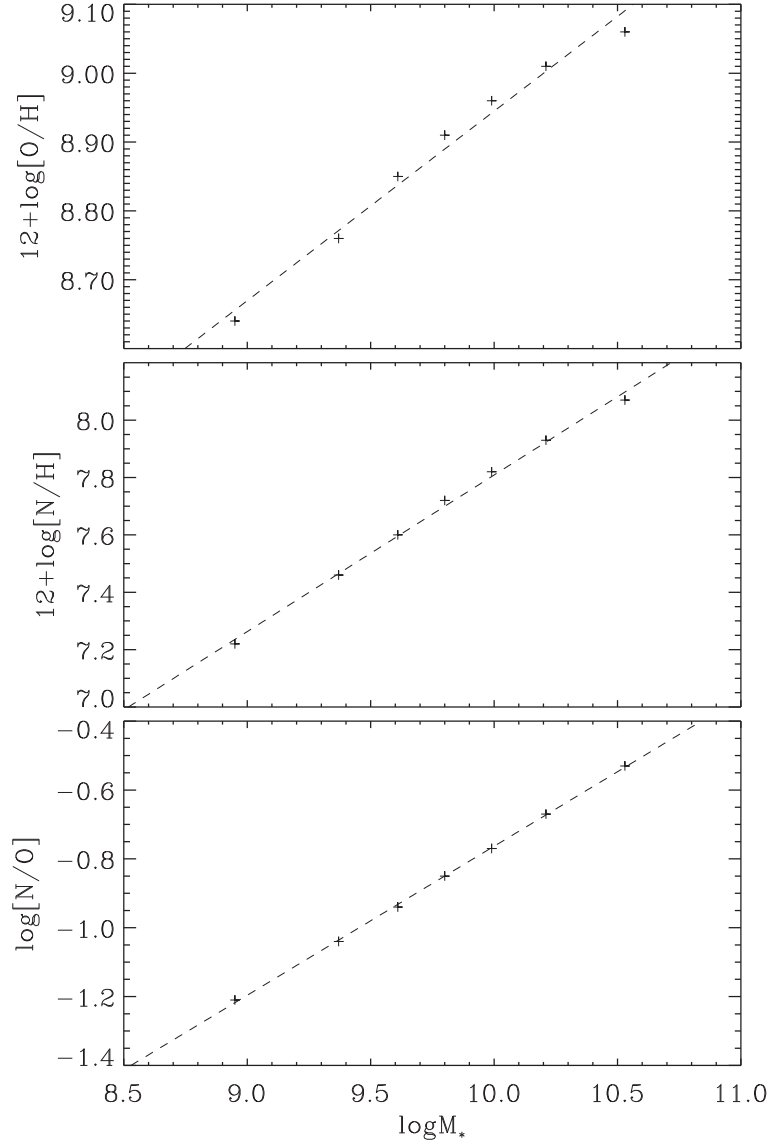


Fig. 12.— Relations between the median values of M_* and $\log \frac{N}{O}$ (bottom panel) $12 + \log \frac{N}{H}$ (middle panel) $12 + \log \frac{O}{H}$ (top panel) for each subsample shown in Fig. 9.

YZW thanks Yanchun Liang for valuable discussions. The anonymous referee is thanked for many constructive comments and suggestions, which allowed us to improve the paper significantly. SNZ acknowledges partial funding support by 973 Program of China under grant 2009CB824800, by the National Natural Science Foundation of China under grant Nos. 11133002 and 10725313, and by the Qianren start-up grant 292012312D1117210.

REFERENCES

- Aller L. H. 1942, *ApJ*, 95, 52
- Alloin D., Collin-Souffrin S., Joly M., Vigroux L. 1979, *A&A*, 78, 200
- Amorín R. O., Pérez-Montero E., Vílchez J. M. 2010, *ApJ*, 715, L128
- Baldwin J. A., Phillips M. M., Terlevich, R., 1981, *PASP*, 93, 5
- Bundy K. et al. 2006, *ApJ*, 651, 120
- Cannon R. D., Croke B. F. W., Bell R. A., Hesser J. E., Stathakis R. A., 1998, *MNRAS*, 298, 601
- Cowie L. L., Songaila A., Hu E. M., Cohen J. G. 1996, *AJ*, 112, 839
- Cowie L. L., Barger A. J. 2008, *ApJ*, 686, 72
- Coziol R., Reyes R. E. C., Considère S., Davoust E., Contini T., 1999, *A&A*, 345, 733
- de Robertis M. M. 1987, *ApJ*, 316, 597;
- Dopita M. A., Evans I. N. 1986, *ApJ*, 307, 431
- Edmunds M. G., Pagel B. E. J. 1984, *MNRAS*, 211, 507
- Erb D. K., Shapley A. E., Pettini M., Steidel C. C., Reddy N. A., Adelberger K. L., 2006, *ApJ*, 644, 813
- Garnett D. R. 1990, *ApJ*, 363, 142
- Gerola H., Seiden P. E., Schulman L.S., 1980, *ApJ*, 242, 517
- Heckman T. M. 2003, *Rev. Mex. Astron. Astrofis. Ser. Conf*, 17, 47
- Henry R. B. C., Edmunds M. G., Köppen J. 2000, *ApJ*, 541, 660

- Kauffmann G. et al. 2003a, MNRAS, 346, 1055
- Kauffmann G. et al. 2003b, MNRAS, 341, 54
- Kelly B. C., 2007, ApJ, 665, 1489
- Kewley L. J., Dopita M. A. 2002, ApJS, 142, 35
- Kewley L. J., Ellison S. L. 2008, ApJ, 681, 1183
- Kobulnicky H. A., Kennicutt R. C., Pizagno J. L. 1999, ApJ, 514, 544.
- Koeppen J., Theis C., Hensler G., 1995, A&A, 296, 99
- Kroupa P. 2001, MNRAS, 322, 231
- Krugel E., Tutukov A. V. 1993, A&A, 275, 416
- Lamareille F. et al. 2009, A&A, 495, 53
- Lara-López M. A., Cepa J., Bongiovanni A., Pérez García A. M., Castañeda H., Fernández L. M., Pović m., Sánchez-Portal M., 2009, A&A, 505, 529
- Lehnert M. D., Heckman T. M. 1996, ApJ, 462, 651
- Liang N., Wu P., Zhang S. N. 2010, Phys. Rev. D, 81, 083518
- Liang N., Xiao W. K., Liu Y., Zhang S. N. 2008, ApJ, 685, 354
- Liang Y-C., Yin S.-Y., Hammer F., Deng L.-C., Flores H., Zhang B. 2006, ApJ, 652, 257
- Lilly S. J., Carollo C. M., Stockton A. 2003, ApJ, 597, 730
- López-Sánchez Á. R., Esteban C. 2010, A&A, 517, A85
- Maeder A. 1992, A&A, 264, 105
- Maiolino R. et al. 2008, A&A, 488, 463
- Mallery R. P. et al. 2007, ApJS, 173, 482
- Marconi G., Matteucci F., Tosi, M. 1994, MNRAS, 270, 35
- McCall M. L., Rybski P.M., Shields G. A. 1985, ApJS, 57, 1
- Moran E. C., Lehnert M. D., Helfand D. J. 1999, ApJ, 526, 649

- Olofsson K. 1995, *A&A*, 293, 652
- Osterbrock D. R. 1989, *Astrophysics of Gaseous Nebulae and Active Galactic Nuclei* (Mill Valley CA: University Science Books)
- Pagel B. E. J. 1986, *PASP*, 98, 1009
- Pagel B. E. J. 1997, *Nucleosynthesis and Chemical Evolution of Galaxies* (Cambridge: Cambridge Univ. Press)
- Pagel B. E. J., Edmunds M. G., Blackwell D. E., Chun M. S., Smith G., 1979, *MNRAS*, 189, 95
- Pagel B. E. J., Simonson E. A., Terlevich R. J., Edmunds M. G. 1992, *MNRAS*, 255, 325
- Peimbert M. 1975, *ARA&A*, 13, 113
- Pérez-Montero E., Contini T. 2009, *MNRAS*, 398, 949
- Pilyugin, L. S., Thuan, T. X. 2011, *ApJ*, 726, L23
- Pilyugin L. S., Thuan T. X., Vílchez J. M. 2003, *A&A*, 397, 487
- Pilyugin L. S., Thuan T. X., Vílchez J. M. 2006, *MNRAS*, 367, 1139
- Pilyugin L. S., Vílchez., Cedrés., Thuan, T. X. 2010, *MNRAS*, 403, 896
- Pilyugin L. S., Lara-López M. A., Grebel E. K., Kehrig C., Zinchenko I. A., López-Sánchez Á. R., Vílchez J. M., Mattsson L., 2013, *MNRAS*, 432, 1217
- Poggianti B. M., Bridges T. J., Komiyama Y., Yagi M., Carter D., Mobasher B., Okamura S., Kashikawa N., 2004, *ApJ*, 601, 197
- Renzini A., Voli, M. 1981, *A&A*, 94, 175
- Salim S. et al. 2007, *ApJS*, 173, 267
- Savaglio S. et al. 2005, *ApJ*, 635, 260
- Skillman E. D., Kennicutt R. C., Jr. 1993, *ApJ*, 411, 655
- Smiljanic R., Barbuy B., de Medeiros J. R., Maeder A., 2006, *A&A*, 449, 655
- Strickland D. K., Ponman T. J., Stevens I. R. 1997, *A&A*, 320, 378
- Thuan T. X., Pilyugin L. S., Zinchenko I. A. 2010, *ApJ*, 712, 1029

- Thurston T. R., Edmunds M. G., Henry R. B. C. 1996, MNRAS, 283, 990
- Torres-Papaqui J. P., Coziol R., Ortega-Minakata R. A., Neri-Larios D. M. 2012, ApJ, 754, 144
- Tremonti, C. A. et al. 2004, ApJ, 613, 898
- van den Hoek L. B., Groenewegen M. A. T. 1997, A&AS, 123, 305
- van Zee, L., Haynes M. P. 2006, ApJ, 636, 214;
- Veilleux S. Osterbrock D. E. 1987, ApJS, 63, 295
- Vila-Costas M. B., Edmunds M. G. 1993, MNRAS, 265, 199
- Wu Y.-Z., Zhao Y.-H., Meng X.-M. 2011, ApJS, 195, 17
- Yin S. Y., Liang Y. C., Hammer F., Brinchmann J., Zhang B., Deng L. C., Flores H., 2007, A&A, 462, 535
- York D. G. et al. 2000, AJ, 120, 1579
- Zahid H. J., Bresolin F., Kewley L. J., Coil A. L., Davé R., 2012, ApJ, 750, 120